Nanoscale

Cite this: *Nanoscale*, 2012, **4**, 6383

www.rsc.org/nanoscale

PAPER

Floral-clustered few-layer graphene nanosheet array as high performance field emitter

Lin Li, Wangning Sun, Shibing Tian, Xiaoxiang Xia, Junjie Li* and Changzhi Gu*

Received 18th June 2012, Accepted 10th August 2012
DOI: 10.1039/c2nr31524f

Graphene sheet is expected to be a highly efficient field emitter due to its unique electrical properties and open surface with sharp edges. However, it is still a tremendous technical challenge to grow and align a graphene sheet in one particular direction to protrude its sharp edges for good field emission. Here, we report an ideal graphene field emitter of flower-like graphene nanosheets grown on a silicon nanocone array, wherein nanocone array guides the alignment of vertical nanosheets and produces high-density sharp edge protrusions on the conical tip. We observe high performance and stable field emission with low turn-on fields from floral-clustered graphene nanosheets. Protrusive sharp edges on the nanocone tip and optimized spacing between clusters both appear to locally enhance the electric field and dramatically increase field emission. Our new graphene emitter design provides a robust approach to the prospect for development of practical electron sources and advanced devices based on graphene field emitters.

Introduction

Most electron emitter applications today take advantage of thermionic emission to generate high-current electron beams for a variety of applications such as X-ray sources, electron microscopes, cathode ray tube (CRT) displays, and microwave amplifiers,[1–3] but some problems still exist such as instability, bulkiness and heat radiated around the device. Therefore, cold cathode emitters attract much attention because they can work at room temperature with a fast turn-on process, and they provide high emission current density at low electric fields while making smaller devices possible and reducing the constraints in material considerations.[4] So far, various low-dimensional nanomaterials have been demonstrated to be candidates for cold cathode emitters, among which the most notable are the carbon nanomaterials—including nanotubes, nanofibers, nanorods, nanocones and nanowalls[5–9]—which have been widely studied to explore their applications as electron sources due to their unique structure with achigh aspect ratio and excellent electronic and mechanical properties. Perhaps of the greatest importance is the very promising carbon nanotube's field emission property, with low turn-on voltage and high emission current far superior to other field emitters, which is also a significant feature of high performance field emitters.

A new carbon nanomaterial, graphene was first prepared in 2004,[10] and has subsequently become an exciting material for research due to its fascinating physical properties. It has attracted immense and persistent interest in its enormous application potential.[11–14] Graphene is a 2-D planar graphitic nanostructure, and its open surface and sharp edge producing a large aspect ratio make it attractive for field electron emission applications. Some recent reports indicate that the turn-on field of flat graphene sheets is very high, on the order of 10^8 V m^{-1},[15] but significant enhancement of graphene's electron field emission can be obtained only in the sharp edges of graphene when an electric field is applied along the sheet because of the reduction of the work function at the edges as compared to the graphene sheet body.[16] Therefore, the growth and alignment of graphene sheets in one particular direction has become a breakthrough much sought after in the development of graphene as a field emitter. Although it is a tremendous technical challenge to grow and align vertical single-layer graphene, technical progress was recently made to prepare vertical few-layer graphene nanosheets by a CVD method.[17–23] Few-layer graphene structures—usually with 3–10 layers—have been extensively studied due to having electrical properties similar to graphene and because they are easy to prepare.[24–28] However, the few-layer graphene sheets reported so far often have uncontrollable morphologies, and their edges are too closely packed, which gives rise to a field screening effect that dramatically hampers the desired increase in field emission. So at this point, controlling the overall morphology and simultaneously optimizing the edge arrangement of an array of vertical few-layer graphene sheets would be a big step toward obtaining a large field enhancement factor, and such material may even have field emission properties quite comparable to those of carbon nanotubes. Therefore, finding a means of utilizing the sharp edge of graphene sheets to design new emission structures is an immediate concern of researchers

Beijing National Laboratory for Condensed Matter Physics, Institution of Physics, Chinese Academy of Sciences, Beijing 100190, China. E-mail: jjli@iphy.ac.cnand; czgu@iphy.ac.cn

investigating graphene as an ideal field emitter for practical applications.

To dramatically improve the field emission properties of vertical few-layer graphene sheets, two aspects should be considered foremost: configuring plenty of vertically aligned sharp edges, and suitably separating the edges from each other to increase the local electrical field and the field enhancement factor. Here, we report a newly designed graphene emitter—a petaloid graphene nanosheet (PGNS) of few layers, grown on a silicon nanocone array (SNCA) by hot-filament chemical vapor deposition (HFCVD) method, in which the nanocone structure functionalizes the graphene nanosheet and serves as a template causing the sharp edges of graphene nanosheets to form a floral-form tip on each cone, yielding a strong tip effect for field emission applications. These as-grown few-layer PGNSs have very sharp edges, and their outermost edge may even be a single layer. In addition, these PGNSs are grown controllably on a SNCA to produce clusters of PGNSs, where the space between clusters is controlled by the periodicity of SNCA and the growth time of PGNSs and hence to optimize the morphology and edge density of PGNS. Indeed, the SCNA greatly enhances the field emission factor of the whole structure. Our results show that the structure is highly efficient and stable in field emission, with a low turn-on field. The combination of abundant protruding sharp edges and optimal spacing between clusters is demonstrated to locally enhance the electric field and dramatically increase field emission. Our design for new graphene emitters provides a robust approach to the development of practical electron sources as well as advanced devices based on graphene field emitters.

Experimental

The silicon nanocone array was fabricated by cryogenic maskless etching in an inductively coupled plasma (ICP) system, in which SF_6 and O_2 were used as etching gas to fabricate Si nanocones. The geometry of Si nanocones, such as height, density or aspect ratio, was modulated through changing the etching parameters. An as-formed silicon nanocone array served as the substrate to grow the few-layer graphene nanosheets by HFCVD. The Ar, H_2 and CH_4 were fed into the HFCVD system with a ratio of 40 : 10 : 1 for the growth of PGNSs. The growth process was carried out under different temperatures from 700 to 1000 °C, and pressure was maintained at 2 kPa in all cases. A positive bias voltage was added on the filament during growth. The bias current was measured with an ammeter.

The morphology and structure and the chemical bond-state of the obtained samples were characterized by scanning electron microscopy (SEM), transmission electron microscopy (TEM), high resolution transmission electron microscopy (HRTEM) (at 200 kV), electron energy loss spectroscopy (EELS) and Raman spectra.

A typical parallel setup was placed in a high vacuum chamber ($\sim 10^{-6}$ Pa), in which the as-prepared sample and an aluminum plate were the cathode and anode, respectively. The distance between the cathode and anode was 300 μm, and testing was done at room temperature. When the applied voltage between cathode and anode was increased, the emission current was recorded using an amperometer.

Results and discussions

The PGNSs are uniformly grown on a silicon nanocone array by HFCVD using CH_4 and H_2. The process of preparing the PGNS samples is detailed in the Experimental section below. Fig. 1a presents a SEM image of a silicone nanocone array fabricated by ICP etching, used as the substrate of PGNSs. Cones are approximately 900 nm in height with a tip radius of less than 10 nm, and their distribution density is about $\sim 3.5 \times 10^9$ cm^{-2}. These nanocones have a very sharp tip geometry, which favors the growth of graphene nanosheets with many sharp edges and with functionalized field emission properties. Fig. 1b shows the morphology of graphene nanosheets grown on SNCAs in Fig. 1a. These graphene nanosheets entirely cover the cone surface and seem to mimic the shapes of flower petals. The petaloid graphene nanosheet clusters are isolated from each other due to the conical array's structure, which effectively optimizes the density of the PGNS array. The high-resolution SEM image shown in Fig. 1c gives a clear view of the edges of PGNSs on the cone tip, and their petaliform edges are very thin, spreading out layer by layer. Compared with vertical graphene nanosheets grown on the flat substrate of silicon wafer, as shown in Fig. 1d, the form of our nanosheets grown on the nanocone array greatly enhances the configuration of both the sharp edges and the large surface areas, which together are very favorable for both the field enhancement factor and the emission site density needed for a good field emitter.

Further structural details of the as-grown graphene nanosheets were acquired from the TEM images, EELS and Raman spectra, as shown in Fig. 2. Fig. 2a is a TEM image of graphene fragments scraped from a PGNS, revealing the very thin sheet structure of graphene. The edges of a graphene nanosheet are shown in a

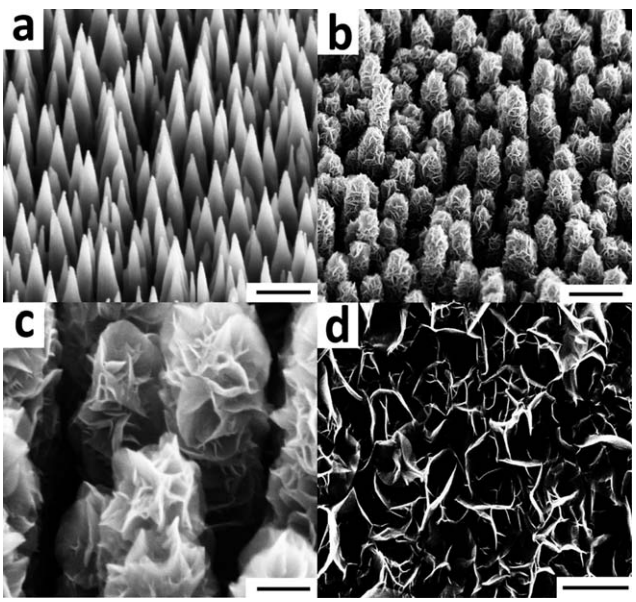

Fig. 1 SEM images of (a) silicon nanocone array, (b) floral-clustered graphene nanosheets grown on a nanocone array with a growth time of 30 min and a bias current of 10 mA, (c) high-resolution image of petaliform graphene nanosheets on a nanocone tip, (d) vertical graphene sheets grown on a flat silicon wafer. The scale bar of (a), (b) and (d) is 1 μm, and the scale bar of (c) is 200 nm.

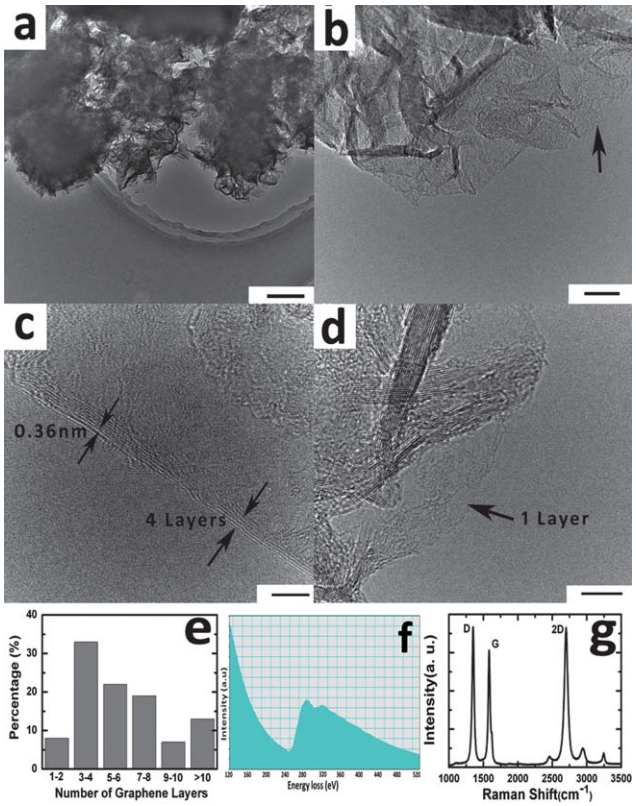

Fig. 2 (a) and (b) TEM images of PGNS (200 nm and 20 nm in scale bar), (c) HRTEM image of PGNS with four layers and (d) monolayer graphene (5 nm in scale bar), (e) layer-number distribution, (f) EELS and (g) Raman spectrum of PGNS samples.

clearer TEM image (Fig. 2b), which distinctly presents the sharp edge with its few layers. Fig. 2c and d are HRTEM images, clearly showing the details of a few-layer graphene nanosheet. In Fig. 2c, the interference fringe of the graphene edge, indicated by arrows, indicates that there are four layers in a nanosheet, and the interlayer spacing is only 0.36 nm, larger than that of typical bulk graphite (0.34 nm), implying a reduction of the van der Waals interaction. Another HRTEM image, Fig. 2d shows monolayer graphene. These TEM images all show with certainty that the as-grown samples are few-layer graphene nanostructures, guaranteeing the sharp edges needed for good field emission ability. Summing up from abundant TEM images, we achieved good distribution of the graphene nanosheet layers, as shown in Fig. 2e. We find that the number of layers in an as-grown graphene nanosheet is almost always fewer than ten, and three- and four-layer nanosheets are the most common. Also, about 8% have only one or two layers. The formation of these nanosheets is heavily influenced by the etching effects of H^+ in the gas species, which limits the interminable growth of the nanosheets in three-dimensional space. The electron energy loss spectroscopy shown in Fig. 2f indicates that the bonding energy is about 320 eV, corresponding to the C–C bond of graphene. Fig. 2g shows the Raman spectrum of our PGNS. In addition to typical D and G peaks, a symmetrical single 2D peak at around 2701 cm is observed, which stems from the second order of the zone-boundary phonons and is closely related to the number of layers in the graphene sheet. The 2D peak is more intense than the G peak, indicating that the petaliform nanostructure is indeed highly organized few-layer graphene. The D peak is related to the disorders and defects of graphene,[29] and the intensity of the D peak relative to the G peak (I_D/I_G) reflects the abundance of defects in this graphene.

The morphology of a PGNS has a very important influence on its electron emission properties and practical field emission applicability. During the CVD growth process, growth temperature, bias current and growth time can all change the morphologies of PGNSs. We prepared samples at different bias levels and growth times while continuing to use an optimum growth temperature of 1000 °C to observe the morphological evolution of PGNSs and understand their growth process. Fig. 3 reveals the influence of the bias current on PGNS growth. In particular, Fig. 3a presents various features of PGNSs at different bias currents. Here, it can be observed that if there is no bias current, the graphene nanosheets grow very sparsely and in irregular orientations. But with a bias current of 10 mA, the graphene nanosheets become well ordered along the electric field, showing that the applied bias voltage is very favorable for the vertical growth of graphene nanosheets. With increasing the bias current, up to 50 mA, the size of graphene nanosheets decreases obviously while these sheets are increasingly close-packed, which markedly reduces the sharpness of the edges and is hence bad for field emission. These morphological changes are closely related to the structure and defects of the nanosheets. Fig. 3b shows the corresponding Raman spectra of PGNSs grown at different bias currents. It is apparent that I_D/I_G increases continually with the increase of bias current, meaning that the bias current

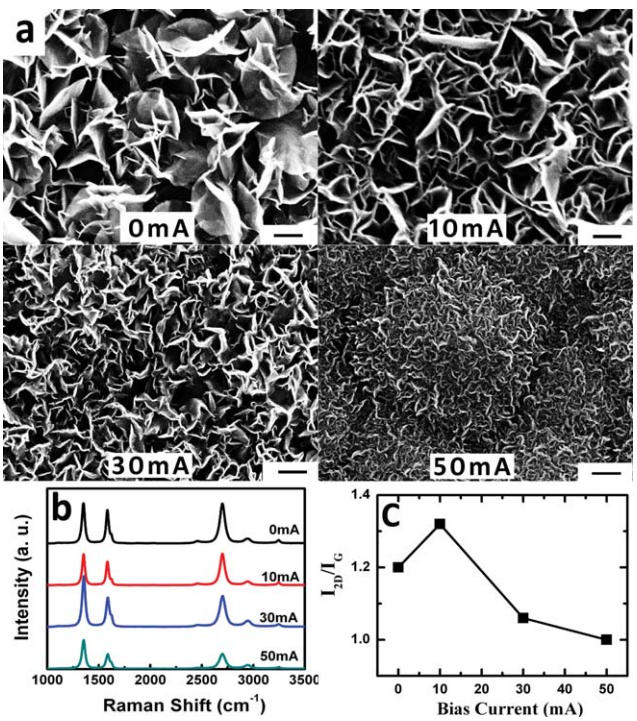

Fig. 3 SEM images and Raman spectra of PGNSs grown for 60 min at different bias currents. (a) SEM images (200 nm in scale bar). (b) Raman spectra of graphene sheets grown at 0, 10, 30 and 50 mA. (c) Change of I_{2D}/I_G with bias current.

contributes to defect formation. The intensity ratio of the 2D peak and G peak (I_{2D}/I_G) is commonly adopted to evaluate the few-layer graphene; graphene with very few layers tends to have a larger I_{2D}/I_G and is in conformity with graphene of quite few layers. The change of I_{2D}/I_G with bias current is showed in Fig. 3c. The highest I_{2D}/I_G (~1.35) is obtained at 10 mA, indicating that this bias favors the growth of high-quality super-thin graphene. Our last increase of the bias current leads to a significant decrease of I_{2D}/I_G, which is due to an increase of the defects at this bias current, the the defects in turn induce the formation of smaller and denser nanosheets.

Fig. 4 shows the evolution of PGNSs with growth time from 5 min to 60 min. In order to obtain high-quality super-thin graphene with a proper density for field emission measurement, we selected a bias current of 10 mA during growth. With increasing the growth time, the size and density of these nanostructures vary dramatically. As growth begins, the petals of PGNSs are very small with a big interval from the silicon nanocone substrate, and then PGNSs grow up slowly while the empty space in the array between PGNS clusters decreases as time passes. After 30 min of growth, a flourishing array of floral-clustered graphene nanosheets with proper spacing between the clusters has been formed. After 60 min, as-grown graphene nanosheets submerge the silicon nanocones to the degree that the location of cones is obscured. The composite nanostructure degenerated to the case that few-layer graphene is grown on the flat surface. Through changing the growth time, we modulated both the PGNSs' features and the amount of open space in the array between PGNSs clusters, which is supposed to tune their field emission properties and obtain excellent field electron emission.

The growth process of few-layer graphene on a silicon nanocone array in a HFCVD system is sketched in Fig. 5. This process has two aspects: (1) the internal stress and external electric field together induce warped and vertical growth of PGNSs, and (2) both the defect-guided nucleation and H^+ etching determine the number of graphene layers. First, a mixed gas of H_2 and CH_4 was brought into the system (Fig. 5a) and decomposed to growth species (CH_x^+) and hydrogen ions (H^+). These growth species are

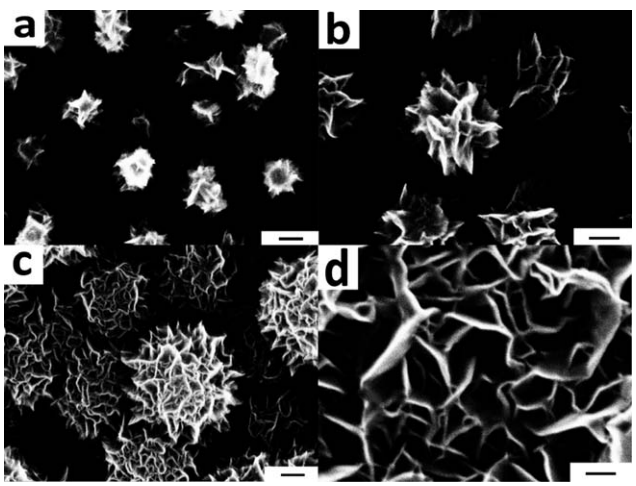

Fig. 4 SEM top-view images of PGNS/SNCAs grown for different durations: (a) 5 min, (b) 10 min, (c) 30 min and (d) 60 min with 100 nm in the scale bar.

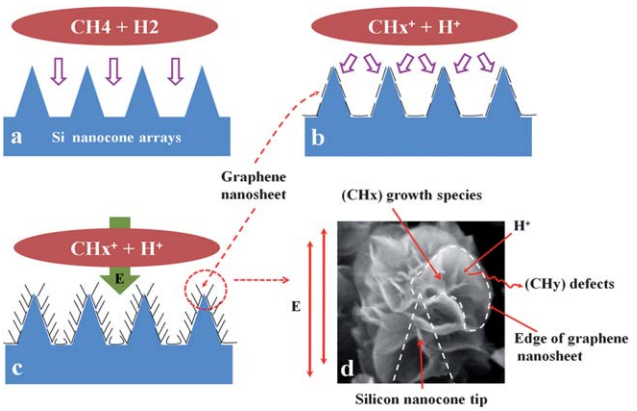

Fig. 5 Schematic diagram of vertical graphene nanosheets growing on silicon nanocones. (a) Silicon nanocones are put into the mixed gas of H_2 and CH_4. (b) The growth species carbon atoms assemble into graphene nanosheets on the substrate surface. (c) Local electric field promotes graphene growth in two dimensional sheets along the direction of electric field. (d) Some defects (CH_y) are dislodged by H^+ etching effects while the growth species (CH_x) are adsorbed for further growth.

some active carbon atoms. At the beginning of the growth, the carbon atoms of the growth species form graphene nanosheets on the substrate surface (Fig. 5b). Additional growth species molecules arrive and diffuse on the surface of the graphene nanosheets and form covalent bonds at the edges of the graphene nanosheets.[30–32] Due to the internal stress, the edges of the graphene warp and stick up, which determines the growth trend of the petaliform nanostructure. At this point, the external electric field induces a local electric field perpendicular to the cone surface, which promotes graphene growth in the two-dimensional sheets along the direction of the electric field (Fig. 5c).[32] Therefore, the edges of the graphene sheets grow into an irregular ring, marked with a dotted line in Fig. 5d. On the other hand, initial defects in the graphene nanosheets come from a thin defective carbon layer for nucleation that can be detected by the Raman spectrum with a D peak and G peak after the duration of the growth. These defects in the defective carbon layer grow by absorbing active carbon atoms. The growth species (CH_x) diffusing on flawed graphene collide with each other continually. These collisions increase the probability of defects capturing the diffusing molecules. Therefore, the defects in graphene capture abundant growth species building up the carbon nanosheets. Along with this defect-guided nucleation and growth, the etching effect of H^+ is also important in the growth process of PGNSs. During the growth, H^+ etches the carbon defects (CH_y) and restrains the nucleation of carbon nanosheets (Fig. 5d). This effect restricts the number of graphene layers. Therefore, the defect-guided nucleation and the etching effect of H^+ determine the number of graphene piles, together.

The field emission properties of PGNS samples grown at a temperature of 1000 °C and a bias current of 10 mA were tested using a parallel-plate measurement configuration in a chamber evacuated to 10^{-6} Pa at room temperature (see method). Fig. 6a shows the emission current density (J) of PGNS/SNCAs, pure silicon nanocones and PGNSs grown on a flat silicon wafer as a function of the applied current (E). It is found that the turn-on electric field (E_{on}, 2.6 V μm^{-1} at 10 μA cm^{-2}) and threshold field

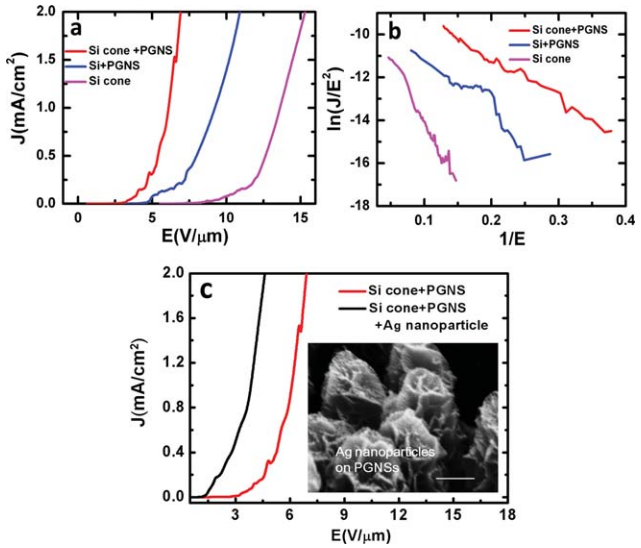

Fig. 6 Field emission properties. (a) *J*–*E* curves and (b) the corresponding $\ln(J/E^2)$–$(1/E)$ curves of PGNS/SNCAs, PGNS/Si and pure silicon nanocones; (c) field emission from PGNS/SNCAs without and with Ag nanoparticles, and inset is the SEM image of a PGNS cluster decorated by Ag nanoparticles (200 nm in the scale bar).

(E_{th}, 5.8 V μm^{-1} at 1 mA cm^{-2}) of the PGNS/SNCAs are significantly lower than those of the as-grown PGNSs/Si (E_{on}, 4.5 V μm^{-1}; E_{th}, 9.2 V μm^{-1}), and pure SNCAs (E_{on}, 7.3 V μm^{-1}, E_{th}, 13.5 V μm^{-1}). It is easy to understand that SNCAs coated by PGNSs have an enhanced electron field emission due to the high conductivity and abundant sharp edges of PGNSs, which together increase both the field emission enhancement factor and the number of effective emission sites. The superior field emission of a PGNS/SNCA compared with PGNSs grown on the silicon wafer is attributed to the conical nanostructures that optimize the PGNS arrays' density and serve as a matrix for the growth of abundant sharp edges. Fig. 6b shows FN plots corresponding to *J*–*E* curves, in which linear FN plots indicate typical field emission behavior.

In order to improve the field emission properties of PGNS/SNCAs, we coated the PGNSs with discrete Ag nanoparticles, as shown in the inset of Fig. 6c. From the *J*–*E* plots of field emission in Fig. 6c, we can observe that the field emission from a coated PGNS/SNCAs is significantly increased, and both its turn-on electric field and its threshold field are lowered still further to 1.15 V and 3.76 V μm^{-1}, which are a little better than the reported superexcellent field emission properties of the carbon-based nanostructure, such as well-aligned carbon nanotubes (1.6 and 5 V μm^{-1}),[33] diamond nanorods (1.3 and 3.9 V μm^{-1})[34] and single-layer graphene films (2.3 and 5.2 V μm^{-1}).[35] Discrete Ag nanoparticles on the PGNSs are unavailable for electrons tunnel through a surface potential–energy barrier during the field emission process due to the similarity of silver's work function (~4.3 eV) and that of few-layer graphene edges (less than 4.7 eV), and thus the change of the work function of graphene induced by Ag nanoparticle introduction may be very little. However, during applying an external electric field, the presence of Ag nanoparticles enhances local electric field distribution around the sharp edges of PGNSs and introduces new field emission sites for launching electrons, all of which enhances the structure's capability for field emission. This enhancement effect induced by metallic nanoparticles is also observed in the field emission from carbon nanotube and graphene decorated by metallic particles.[36–38]

In addition, the morphology of an emitter is a very important factor influencing its electron emission ability because it is closely related to the field enhancement factor (β). Larger β means larger local electric fields at the emitter tips and is beneficial for electron emission. The morphologies of PGNS/SNCAs can be modulated by changing the growth time in the fixed substrate of the silicon nanocone arrays, as given in Fig. 4, and their effects on the field emission properties are shown in Fig. 7a. The sample grown for 30 min shows the best field emission properties, and either too short (5 min) or long growth (60 min) time lowers the electron emission ability of PGNS/SNCAs. The $\ln(J/E^2)$–$(1/E)$ curves shown in Fig. 7b also reveal the same tendency; their near-linear plots indicate FN type field emission behavior. With the FN plot slope and the reported work function of few-layer graphene (4.7ev), β of the samples grown for different times can be determined, as shown in Fig. 7c. We found that the sample grown for 30 min has the highest β of ~3788, and has the lowest turn-on electric field and threshold field among all samples grown for different times, indicating this morphology is optimal for field electron emission. The sample grown for 5 min has a β (~1766) similar to bare silicon nanocones due to its light coating of graphene nanosheets. Enhanced growth time can modulate the morphology of PGNS/SNCAs while β is also increased, but excessive growth time (60 min) reduces β markedly because closely packed nanosheets already entirely cover the cones, which greatly hampers the nanocones' enhancement of field emission and gives rise to field screening, reducing electric field localization. The observed effects of morphology on a PGNS/SNCA's field emission suggest that the presence of silicon nanocones is not only a critical factor in tuning field emission, but the nanosheets' edge density and the clusters' spacing also play important roles. It is now clear that the excellent field emission properties of PGNS/SNCAs should be attributed to (1) the increased number

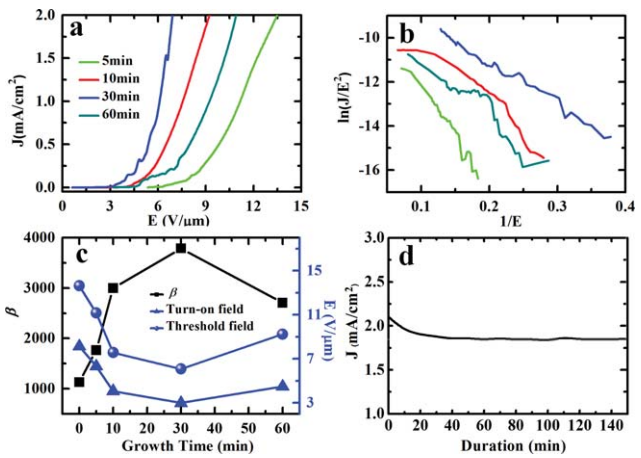

Fig. 7 Field emission properties of PGNSs: (a) *J*–*E* curves and (b) $\ln(J/E^2)$–$(1/E)$ curves of PGNSs grown for different times; (c) change of turn-on electric field (10 μA cm^{-2}), threshold field (1 mA cm^{-2}) and β of PGNSs with growth time; (d) stability of field emission current.

of effective emission sites at the abundant sharp edges of graphene nanosheets, (2) the higher aspect ratio of the Si nanocone substrate for high β, and (3) optimal spacing between clusters, which reduces the field screening effect.

In particular, we tested the stability of PGNS/SNCAs' field emission current around ~2.0 mA cm^{-2} for over 2 h, as shown in Fig. 7d. It is found that at the beginning the current density falls off obviously, and then gradually declines to ~1.85 mA cm^{-2} after about 30 min. With the emission process proceeding, the emission current gradually becomes stable. The whole test period of over two hours showed current degradation of ~7%, which is due to Joule heating from graphene nanosheet emitter which reduces the number of emission sites. These stable and outstanding field emission properties of PGNS/SNCAs, with a lower turn-on and threshold field, are very favorable for practical field emission applications.

Conclusions

We report a new graphene emitter–petaloid graphene nanosheet clusters grown on an array of silicon nanocones, showing a low turn-on field (1.15 V μm^{-1}) with a rapid increase in emission current density. This great enhancement of field emission properties is attributed to two factors: (1) the growth on a nanocone array template enhances the sharp edges effect of graphene nanosheets, which in turn increases the local field enhancement factor, and (2) the design of the nanocone array optimizes the array density of these clusters of sharp edges, reducing the field screening effect. In addition, we found that separate Ag-nanoparticles decorated on the edges of the graphene can further increase the structure's electron emission ability due to the particles' local field enhancement. These results demonstrate that the as-designed floral-clustered graphene nanosheet emitter is an excellent cold electron emission source. Such clusters of petaloid graphene nanosheets may open up a new and interesting subject for basic physics as well as providing a design component for novel applications in areas such as nanolithography, vacuum electronics, and electron optic devices.

Acknowledgements

This work was supported by the National Natural Science Foundation of China (Grant no. 91023041, 50825206, 10834012, 11174362), the National Basic Research Program of China (Grant no.2009CB930502) and the Knowledge Innovation Project of CAS (Grant no. KJCX2-EW-W02).

References

1 K. L. Jensen, *Phys. Plasmas*, 1999, **6**, 2241–2253.
2 C. Hernandez-Garcia, M. L. Stutzman and P. G. O'Shea, *Phys. Today*, 2008, **61**, 44–49.
3 R. J. Umstattd, in *Modern Microwave and Millimeter-Wave Power Electronics*, ed. R. J. Barker, J. H. Booske, N. C. Luhmann and G. S. Nusionovich, IEEE Press, Piscataway, NJ, 2005, pp. 393–444.
4 J. M. Bonard, J. P. Salvetat, T. Stockli, L. Forro and A. Chatelain, *Appl. Phys. A: Mater. Sci. Process.*, 1999, **69**, 245–254.
5 S. S. Fan, M. G. Chapline, N. R. Franklin, T. W. Tombler, A. M. Cassell and H. J. Dai, *Science*, 1999, **283**, 512–515.
6 C. H. Weng, K. C. Leou, H. W. Wei, Z. Y. Juang, M. T. Wei, C. H. Tung and C. H. Tsai, *Appl. Phys. Lett.*, 2004, **85**, 4732–4734.
7 R. Che, M. Takeguchi, M. Shimojo and K. Furuya, *J. Phys. Conf. Ser.*, 2007, **61**, 200–204.
8 L. R. Baylor, V. I. Merkulov, E. D. Ellis, M. A. Guillorn, D. H. Lowndes, A. V. Melechko, M. L. Simpson and J. H. Whealton, *J. Appl. Phys.*, 2002, **91**, 4602–4606.
9 Y. H. Wu, B. J. Yang, B. Y. Zong, H. Sun, Z. X. Shen and Y. P. Feng, *J. Mater. Chem.*, 2004, **14**, 469–477.
10 K. S. Novoselov, A. K. Geim, S. V. Morozov, D. Jiang, Y. Zhang, S. V. Dubonos, I. V. Grigorieva and A. A. Firsov, *Science*, 2004, **306**, 666–669.
11 A. K. Geim and K. S. Novoselov, *Nat. Mater.*, 2007, **6**, 183–191.
12 T. Seyller, A. Bostwick, K. V. Emtsev, K. Horn, L. Ley, J. L. McChesney, T. Ohta, J. D. Riley, E. Rotenberg and F. Speck, *Phys. Status Solidi B*, 2008, **245**, 1436–1446.
13 C. N. R. Rao, A. K. Sood, K. S. Subrahmanyam and A. Govindaraj, *Angew. Chem., Int. Ed.*, 2009, **48**, 7752–7777.
14 S. Park and R. S. Ruoff, *Nat. Nanotechnol.*, 2009, **4**, 217–224.
15 S. Santandrea, F. Giubileo, V. Grossi, S. Santucci, M. Passacantando, T. Schroeder, G. Lupina and A. Di Bartolomeo, *Appl. Phys. Lett.*, 2011, **98**, 163109–163103.
16 H. Yamaguchi, K. Murakami, G. Eda, T. Fujita, P. Guan, W. Wang, C. Gong, J. Boisse, S. Miller, M. Acik, K. Cho, Y. J. Chabal, M. Chen, F. Wakaya and M. Takai, *ACS Nano*, 2011, **5**, 4945–4952.
17 A. Malesevic, R. Kemps, A. Vanhulsel, M. P. Chowdhury, A. Volodin and C. V. Haesendonck, *J. Appl. Phys.*, 2008, **104**, 084301.
18 J. L. Qi, X. Wang, W. T. Zheng, H. W. Tian, C. Q. Hu and Y. S. Peng, *J. Phys. D: Appl. Phys.*, 2010, **43**, 055302.
19 P. W. Sutter, J. I. Flege and E. Sutter, *Nat. Mater.*, 2008, **7**, 406–411.
20 K. S. Kim, Y. Zhao, H. Jang, S. Y. Lee, J. M. Kim, J. H. Ahn, P. Kim, J. Y. Choi and B. H. Hong, *Nature*, 2009, **457**, 706–710.
21 A. Reina, X. T. Jia, J. Ho, D. Nezich, H. B. Son, V. Bulovic, M. S. Dresselhaus and J. Kong, *Nano Lett.*, 2009, **9**, 30–35.
22 X. S. Li, W. W. Cai, J. H. An, S. Kim, J. Nah, D. X. Yang, R. Piner, A. Velamakanni, I. Jung, E. Tutuc, S. K. Banerjee, L. Colombo and R. S. Ruoff, *Science*, 2009, **324**, 1312–1314.
23 A. Dato, V. Radmilovic, Z. H. Lee, J. Phillips and M. Frenklach, *Nano Lett.*, 2008, **8**, 2012–2016.
24 F. Shoushan, L. Liang and L. Ming, *Nanotechnology*, 2003, **14**, 1118–1123.
25 A. C. Ferrari, J. C. Meyer, V. Scardaci, C. Casiraghi, M. Lazzeri, F. Mauri, S. Piscanec, D. Jiang, K. S. Novoselov and S. Roth, *Phys. Rev. Lett.*, 2006, **97**, 187401.
26 S. Gilje, S. Han, M. Wang, K. L. Wang and R. B. Kaner, *Nano Lett.*, 2007, **7**, 3394–3398.
27 L. C. Isett and J. M. Blakely, *Surf. Sci.*, 1976, **58**, 397–414.
28 A. Srivastava, C. Galande, L. Ci, L. Song, C. Rai, D. Jariwala, K. F. Kelly and P. M. Ajayan, *Chem. Mater.*, 2010, **22**, 3457–3461.
29 Y. Wang, D. C. Alsmeyer and R. L. McCreery, *Chem. Mater.*, 1990, **2**, 557–563.
30 Y. H. Lee, S. G. Kim and D. Tománek, *Phys. Rev. Lett.*, 1997, **78**, 2393–2396.
31 O. A. Louchev, Y. Sato and H. Kanda, *Appl. Phys. Lett.*, 2002, **80**, 2752–2754.
32 M. Y. Zhu, J. J. Wang, B. C. Holloway, R. A. Outlaw, X. Zhao, K. Hou, V. Shutthananhdan and D. M. Manos, *Carbon*, 2007, **45**, 2229–2234.
33 H. Murakami, M. Hirakawa, C. Tanaka and H. Yamakawa, *Appl. Phys. Lett.*, 2000, **76**, 1776–1778.
34 N. G. Shang, P. Papakonstantinou, P. Wang, A. Zakharov, U. Palnitkar, I. N. Lin, M. Chu and A. Stamboulis, *ACS Nano*, 2009, **3**, 1032–1038.
35 Z. S. Wu, S. F. Pei, W. C. Ren, D. M. Tang, L. B. Gao, B. L. Liu, F. Li, C. Liu and H. M. Cheng, *Adv. Mater.*, 2009, **21**, 1756–1760.
36 Y. R. Chen, H. Jiang, D. B. Li, H. Song, Z. M. Li, X. J. Sun, G. Q. Miaoand and H. F. Zhao, *Nanoscale Res. Lett.*, 2011, **6**, 537 (1–8).
37 J. Y. Pan, C. Y. Chen, Y. L. Gao and C. C. Zhu, *Displays*, 2009, **30**, 114–119.
38 T. T. Baby and S. Ramaprabhu, *J. Appl. Phys.*, 2012, **111**, 034311 (1–5).

